Reconstruction of a persistent random walk from exit time distributions

Pak-Wing Fok* and Qunhui Han

Department of Mathematical Sciences, University of Delaware, Newark, DE 19716, USA
*Corresponding author: pakwing@udel.edu

and

Tom Chou

Departments of Biomathematics and Mathematics, UCLA, Los Angeles, CA 90095, USA

In this paper, we study the inverse problem of reconstructing the spatially dependent transition rate $F(x)$ of a 1D Broadwell process from exit time distributions. In such a process, an advecting particle is assumed to undergo transitions between states with constant positive $(+v)$ and negative $(-v)$ velocities. The goal is to reconstruct the transition rate function $F(x)$ from the exit time distributions out of a finite interval. Using the associated backward equation, we compute the distribution of exit times and its Laplace transform, given a fixed starting position and velocity. We propose two methods (called 't' and 's') for finding $F(x)$. In both methods, we represent $F(x)$ as a linear combination of polynomials and repeatedly solve the backward equation to minimize the difference between its solution and given first exit time data. In the t-method, we work in the time domain, using exit times directly and leveraging a novel series solution for the exit time distribution. In the s-method, we work with the Laplace-transformed equation and Laplace-transformed exit times. Noisy data are generated using a custom-designed algorithm to simulate the trajectories of a Broadwell process. In most cases, we can find four coefficients to within $O(10^{-1})$ accuracy from $O(10^4)$ exit times, with the t-method slightly outperforming the s-method. We also explore the effectiveness of our algorithms for a fixed number of exit times under different advection speeds and find that optimal reconstruction occurs when $v = O(1)$.

Keywords: random walk; inverse problem; Broadwell process; telegrapher's equation.

1. Introduction

Inverse problems arise in many applications such as medical imaging (Arridge, 1999), high-energy particle physics (Novikov, 1994) and seismology (de Hoop *et al.*, 2009). Most of these applications involve measurement of waves at the boundary of a domain; from this boundary data, one may wish to reconstruct spatially dependent properties within the domain such as the density and/or wave speed. However, there have been fewer successful applications where the underlying physics involves an intrinsic random process. The corresponding 'boundary data' for stochastic inverse problems are probability fluxes or exit time distributions. The types of stochastic inverse problems we are concerned with in this paper involve inferring the parameters of a stochastic process from such a distribution.

One example of such a stochastic inverse problem arises in the reconstruction of bond potentials from rupture time distributions (Dudko, 2009; Freund, 2009; Hummer & Szabo, 2003). In force spectroscopy experiments, an increasing force is applied across a macromolecular bond until it ruptures. Because of thermal fluctuations, the rupture force is a random variable; thus, the goal is to infer properties of the bond potential from the *distribution* of rupture forces. Stochastic inverse problems also commonly arise in diffuse optical tomography (Arridge, 1999; Arridge & Hebden, 1997). In all

these applications, the exit time distribution of a Brownian motion leaving a finite interval is measured, and one wishes to reconstruct the drift and/or diffusion function.

While Brownian motion is a canonical stochastic model, the inverse problem associated with Brownian motion is ill-posed (Bal & Chou, 2003; Fok & Chou, 2010) and motivates the study of stochastic exit time problems based on other types of random walks. Ill-posedness is a trademark of many inverse problems. A problem is *well-posed* if a solution exists, is unique and depends continuously on the data. Otherwise the problem is *ill-posed*. At present, issues of existence and uniqueness of spatially dependent parameters for random walks are generally not well established, although some important results for Brownian motions can be found in Bal & Chou (2003).

In this paper, we generalize the study of Brownian inverse problems by focusing on a class of persistent random walk models called Broadwell processes (Broadwell, 1964a,b; Christlieb *et al.*, 2004; Goldstein, 1951; Masoliver & Weiss, 1994). In a Broadwell process, a particle randomly interconverts ('flips') between multiple states, with each state associated with a particular velocity. The Broadwell process has the desirable property that it interpolates between a ballistic and diffusive motion (Bicout, 1997; Fok *et al.*, 2008): the time between transitions decreases as the flip rate increases, but increases as the flip rate decreases. The Broadwell model opens the analysis of the inverse problem for these two types of limiting processes; studying the inverse Broadwell problem may therefore provide insight into the important, strictly diffusive problem. We shall focus on the constant speed Broadwell process, assuming that transition probabilities that are spatially dependent and that the particle takes only two states associated with a positive and negative velocity. From the distribution of exit times out of a finite interval, our goal is to find the transition probability ('flip-rate') function.

Accurately simulating the exit times of a Brownian motion can be quite involved although reliable methods do exist; see Giraudo & Sacerdote (1999), Giraudo *et al.* (2001), Mannella & Palleschi (1989) and Taillefumier & Magnasco (2010), for example. Nevertheless, one important advantage of studying the Broadwell model is the ease with which it can be simulated. Accurate simulations are critical for comparisons between reconstructed flip-rate functions and the underlying target functions that produced the exit data. When generating the exit time distribution from our simulations, the only source of error (besides round-off) stems from using a finite number of realizations.

The outline of this paper is as follows. In Section 1.1, we present the backward Kolmogorov equation (BKE) for the two-state Broadwell problem parametrized by a spatially dependent (but state-symmetric) transition rate and a constant speed. We also state the inverse problem of reconstructing the flip-rate function from the exit time distributions. The associated optimization problem involves minimizing the distance between the solution of the BKE and the exit time data (derived from simulations or from the solution of the BKE with a given flip rate function). In Section 2, we discuss the numerical aspects of our work. In particular, we present two reconstruction methods. The first involves minimizing the difference between the solution to the BKE and the target data in the time domain. The second involves minimizing the difference between the Laplace-transformed solution of the BKE and transformed exit time data. We also explain the simulation of Broadwell random walkers to test our reconstruction protocols. In Section 3, we present the results of our reconstruction using noisy data and compare the two methods. We show that, for a finite number of exit times, the most reliable reconstruction of the flip rate occurs at an intermediate advection speed, no matter which method is used. In Section 4, we discuss general implications of our results and summarize our findings.

1.1 *Two-state model and statement of inverse problem*

A two-state Broadwell model describes a particle that can take one of two states. Initially, the particle is at position x and in state $i \in \{1, 2\}$. The particle advects within an interval $(-L/2, L/2)$ with velocity $+v$

if $i = 1$ and $-v$ if $i = 2$. While advecting, the particle may change state with probability $F(y)dt$ within time interval $(t, t + dt)$, where y is the current particle position.

Let $w(t \mid x, 1, 0) \equiv w_1(x, t)$ and $w(t \mid x, 2, 0) = w_2(x, t)$ be the exit time distributions conditioned on the particle initially being at position x and having a positive $(+v)$ and negative $(-v)$ velocity, respectively. Then, the exit time distributions satisfy

$$\frac{\partial w_1}{\partial t} = v \frac{\partial w_1}{\partial x} + F(x)(w_2 - w_1), \tag{1}$$

$$\frac{\partial w_2}{\partial t} = -v \frac{\partial w_2}{\partial x} + F(x)(w_1 - w_2), \tag{2}$$

subject to initial conditions

$$w_1(x, 0) = 0, \quad w_2(x, 0) = 0, \tag{3}$$

and boundary conditions

$$w_1(x = L/2, t) = \delta(t), \quad w_2(x = -L/2, t) = \delta(t). \tag{4}$$

A full derivation of the backward equation for the exit time distribution for a general K-state Broadwell process (of which (1–4) are a special case) can be found in Appendix A.

Given $F(x)$, one can solve (1–4) (the 'forward problem') to find $w_1(x, t)$ and $w_2(x, t)$ for all $-L/2 < x < L/2$ and $t > 0$. Note that (1) and (2) constitute Kolmogorov's backward equations for the exit time distributions, and that solving this backward equation defines the *forward* problem for computing $w_1(x, t), w_2(x, t)$ from a known $F(x)$. However, in this paper we are interested in the *inverse* problem.

Problem statement: Consider (1–4). Given a known, fixed $-L/2 < x_0 < L/2$, a known velocity $v > 0$ and exit time distributions $w_1(x_0, t)$ and $w_2(x_0, t)$ for $t > 0$, find $F(x) \in C(-L/2, L/2)$.

In practice, the exit time distributions could come from directly simulating a Broadwell process or from a single solution of the forward problem. For particles that initially advect with velocities $+v$ and $-v$, we refer to associated exit time distributions $w_{1,\text{data}}(x_0, t)$ and $w_{2,\text{data}}(x_0, t)$, respectively; note that $w_{1,\text{data}}(x_0, t)$ and $w_{2,\text{data}}(x_0, t)$ may or may not be noisy. We give details on how $w_{1,\text{data}}$ and $w_{1,\text{data}}$ are computed in Section 2.2.

Unfortunately, (1–4) are not useful in practice for inferring $F(x)$ because the solutions are highly singular. Related quantities that are more regular and whose governing equations are more amenable to numerical methods are the cumulative density functions (CDFs) and Laplace-transformed probability density functions (PDFs). We now give explicit forms for these equations since we make frequent use of them later on.

The CDFs are related to the PDFs by $W_{1,2}(x, t) = \int_0^t w_{1,2}(x, t') \, dt'$. Therefore, upon integrating (1) and (2) in time, we find

$$\frac{\partial W_1}{\partial t} - v \frac{\partial W_1}{\partial x} = F(x)(W_2 - W_1), \tag{5}$$

$$\frac{\partial W_2}{\partial t} + v \frac{\partial W_2}{\partial x} = F(x)(W_1 - W_2), \tag{6}$$

subject to the boundary conditions

$$W_1(L/2, t) = H(t), \quad W_2(-L/2, t) = H(t), \tag{7}$$

and initial conditions

$$W_1(x, 0) = 0, \quad W_2(x, 0) = 0. \tag{8}$$

In (7), $H(t)$ is the Heaviside step function satisfying $H(t) = 1$ if $t > 0$ and $H(t) = 0$ if $t \leqslant 0$. The corresponding inverse problem is to find $F(x) \in C(-L/2, L/2)$ given $-L/2 < x_0 < L/2$, v and $W_{j,\mathrm{data}}(x_0, t) = \int_0^t w_{j,\mathrm{data}}(x_0, t')\, dt'$ for $t > 0$ and $j = 1, 2$. Alternatively, we can also take Laplace transforms of (1) and (2) to find

$$s\tilde{w}_1(x, s) = v\frac{\partial \tilde{w}_1}{\partial x} + F(x)(\tilde{w}_2 - \tilde{w}_1), \tag{9}$$

$$s\tilde{w}_2(x, s) = -v\frac{\partial \tilde{w}_2}{\partial x} + F(x)(\tilde{w}_1 - \tilde{w}_2), \tag{10}$$

subject to boundary conditions

$$\tilde{w}_1(x = L/2, s) = 1, \quad \tilde{w}_2(x = -L/2, s) = 1. \tag{11}$$

The corresponding inverse problem is to find $F(x) \in C(-L/2, L/2)$ given $-L/2 < x_0 < L/2$, v and $\tilde{w}_{j,\mathrm{data}}(x_0, s)$ for $s > 0$ and $j = 1, 2$.

2. Algorithms for reconstruction

This section is divided into three parts. First, we give details on solving the forward problems (9–11) and (5–8). Then we explain how to generate noisy data by directly simulating a Broadwell process with a spatially dependent flip rate. Finally, we discuss a projection method to solve the inverse problem.

2.1   *Solution to the forward problems*

Solution to (9–11): Our method for finding $\tilde{w}_1(x_0, s)$ and $\tilde{w}_2(x_0, s)$ from (9–11) is based on solving the boundary value problem using a pseudospectral method (Trefethen, 2000) for different values of $s \geqslant 0$; see Algorithm 1. The solutions $\tilde{w}_{1,2}(x_0, s)$ are always infinitely differentiable, monotonically decreasing functions in s that $\to 0$ as $s \to \infty$.

Algorithm 1 Algorithm for solving the forward problem (9–11).

1: Require: flip rate function $F(x)$, velocity $v > 0$, interval size L, starting position $-L/2 < x_0 < L/2$ and integer $N \gg 1$.
2: **for** $i = 1, 2, \ldots, N$ **do**
3:     let $\xi_i = (i - 1)/N$ and $s_i = \xi_i/(1 - \xi_i)$.
4:     With $s = s_i$, solve (9–11) using a pseudospectral discretization (Trefethen, 2000) in x.
5:     Interpolate the solution at $x = x_0$ to find $\tilde{w}_1(x_0, s_i)$ and $\tilde{w}_2(x_0, s_i)$.
6: **end for**
7: Output: Laplace Transformed exit time distributions $\tilde{w}_1(x_0, s_i)$ and $\tilde{w}_2(x_0, s_i)$, $i = 1, \ldots, N$.

Solution to (5–8): In contrast to $\tilde{w}_{1,2}(x_0, s)$, the solutions $W_{1,2}(x, t)$ contain jump discontinuities that propagate into the domain of solution with velocity $\mp v$: the jump discontinuity in $W_1(x, t)$ ($W_2(x, t)$) propagates along the characteristic line $t = -x/v + L/(2v)$ ($t = +x/v + L/(2v)$). This behaviour in the singularities is illustrated by the following theorem which uses an eigenfunction expansion to construct an explicit solution to (5–8).

THEOREM 1 (Series solution to the forward problem (5–8)) For $0 < t < L/v$, the solution to (5–8) is

$$W_1(x, t) = a_1(x)H[t + x/v - L/(2v)] + Z_1(x, t), \tag{12}$$

$$W_2(x, t) = a_2(x)H[t - x/v - L/(2v)] + Z_2(x, t), \tag{13}$$

where $H[\cdot]$ is the Heaviside step function and $Z_{1,2}(x, t)$ are continuous functions given by the series

$$\mathbf{Z}(x, t) = -\sum_{m=1}^{\infty} \frac{\mathbf{u}_m(x)}{s_m D_m}[h_m^{(1)}(t) + h_m^{(2)}(t)], \tag{14}$$

where

$$h_m^{(1)}(t) = \int_{-L/2}^{-L/2+vt} p_m^{(1)*}(y)a_2(y)F(y)(1 - e^{(t-y/v-L/(2v))s_m}) \, dy, \tag{15}$$

$$h_m^{(2)}(t) = \int_{L/2-vt}^{L/2} p_m^{(2)*}(y)a_1(y)F(y)(1 - e^{(t+y/v-L/(2v))s_m}) \, dy, \tag{16}$$

$$a_1(x) = \exp\left[-\frac{1}{v}\int_x^{L/2} F(x') \, dx'\right], \tag{17}$$

$$a_2(x) = \exp\left[-\frac{1}{v}\int_{-L/2}^x F(x') \, dx'\right], \tag{18}$$

$$D_m = \langle \mathbf{p}_m(x), \mathbf{u}_m(x) \rangle = \int_{-L/2}^{L/2} \mathbf{p}_m^*(x)\mathbf{u}_m(x) \, dx. \tag{19}$$

In (14), $s_m \in \mathbb{C}$ and $\mathbf{u}_m(x) \in \mathbb{C}^2$ are the eigenvalues and eigenfunctions of $\mathbf{A}$ where

$$\mathbf{A}\begin{pmatrix} u_1 \\ u_2 \end{pmatrix} = \left\{\begin{bmatrix} v\dfrac{d}{dx} & 0 \\ 0 & -v\dfrac{d}{dx} \end{bmatrix} + F(x)\begin{bmatrix} -1 & 1 \\ 1 & -1 \end{bmatrix}\right\}\begin{pmatrix} u_1(x) \\ u_2(x) \end{pmatrix}, \tag{20}$$

along with the boundary conditions $u_1(L/2) = u_2(-L/2) = 0$. Here $\mathbf{p}_m(x) = [p_m^{(1)}(x), p_m^{(2)}(x)]^{\mathrm{T}}$ are the eigenfunctions of the adjoint operator $\mathbf{A}^*$.

We now discuss the behaviour of the solutions $W_{1,2}(x, t)$ in light of (12–13) and defer the proof of the theorem to the end of this section. From (12) and (13), it is clear that discontinuities in the boundary conditions (7) propagate into the interior. In Fig. 1(a), W_1 is discontinuous on the diagonal line separating A, C and B, D, while W_2 is discontinuous on the line separating A, D and B, C. Because the
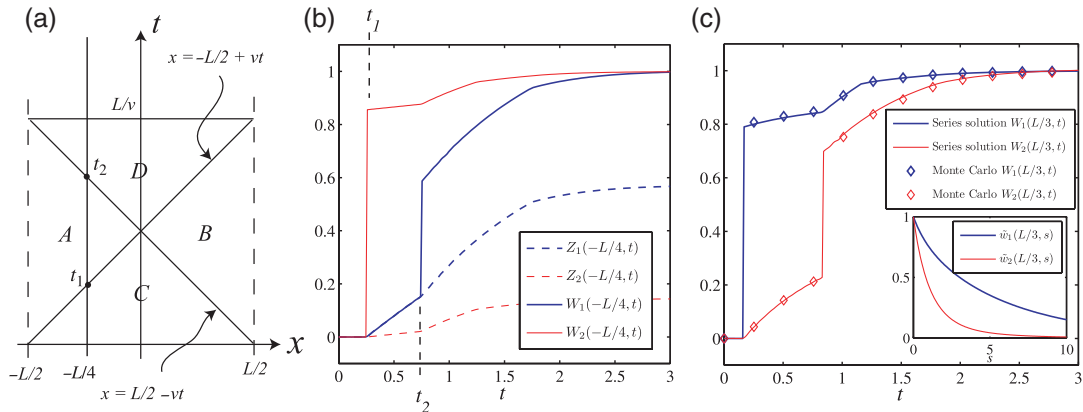
FIG. 1. (a) Propagation of discontinuities of (1–4) in the x–t plane. The solution $w_1(x,t)$ is formally infinite on $x = L/2 - vt$, while $w_2(x,t)$ is infinite on $x = -L/2 + vt$. These singularities give rise to discontinuities in W_1 and W_2 that can be seen in (b, c). (b) Numerical computation of cumulative density functions (CDFs) $W_{1,2}(x_0 = -L/4, t)$ computed through (14) and Algorithm 2 using 101 Chebyshev grid points and 51 eigenfunctions $\mathbf{u}_1, \mathbf{u}_2, \ldots, \mathbf{u}_{51}$. (c) Numerical computation of CDFs $W_{1,2}(x_0 = L/3, t)$ (solid) along with results from Monte Carlo simulations (diamond). Inset shows Laplace-transformed probability densities $\tilde{w}_{1,2}(x_0 = L/3, s)$. Common parameters in (b, c) are $v = 1$, $F(y) = 1 + y$ and $L = 1$.

hyperbolic system (5–8) has a finite wave speed $v > 0$, region C is outside the region of influence of the disturbances originating at $(x, t) = (L/2, 0)$ and $(-L/2, 0)$ and we expect that $W_1(x, t) = W_2(x, t) = 0$ in C. This behaviour is confirmed in Fig. 1(b) which shows the cumulative distribution functions $W_{1,2}(x = -L/4, t)$ calculated using (12–14). The function $W_1(-L/4, t)$ has a discontinuous derivative at $t_1 = L/(4v)$ and a jump discontinuity at $t_2 = 3L/(4v)$ while $W_2(-L/4, t)$ has a jump discontinuity at t_1 and a discontinuous derivative at t_2. Figure 1(c) shows CDFs evaluated at $x_0 = L/3$. The inset shows associated Laplace-transformed PDFs $\tilde{w}_1(L/3, s)$ and $\tilde{w}_2(L/3, s)$, found by solving (9–11) using Algorithm 1. CDFs from Monte Carlo simulations are superposed to validate our numerical method; details of how these simulations are performed are described in Section 2.2.

The expansions (12–13) in Theorem 1 are commonly used to analyse seismic waves (de Hoop *et al.*, 2009; Sacks & Symes, 1987; Symes, 1991) and form the basis of our numerical method for the forward problem in t; see Algorithm 2. Numerically, the CDFs $W_{1,2}$ are computed by taking a finite number of terms in (14) and adding on a step discontinuity at $t = \mp x/v + L/(2v)$ with strength given by (17) and (18). A pseudo-spectral collocation method on a Chebyshev grid was used to find the eigenvectors $\mathbf{u}_j$ and Clenshaw–Curtis quadrature (Trefethen, 2000) was used to quickly evaluate the integrals (15) and (16) for $0 < t < L/v$. The strength of this numerical method is that no integration in time is required to find $W_{1,2}(x_0, t)$ and the method allows quick evaluation of the CDFs at one fixed value of $x = x_0$. Its weakness is that many terms are usually required ($\gtrsim 100$) in the expansion to obtain accurate results when x_0 is close to $\pm L/2$. Furthermore, we found that when $x_0 = \pm L/2$, the expansion (14) converged to a discontinuous function, giving $W_{1,2}(x_0, t) > 1$ as $t \to \infty$; hence, the properties of the series (14) still require further investigation at the domain boundaries.

Another important reason for separating out W_1 and W_2 into continuous and discontinuous components is to avoid Gibbs oscillations when solving for $\mathbf{Z}(x, t)$ in terms of superpositions of eigenfunctions $\mathbf{u}_n$. These oscillations would introduce large errors into the solution to the forward problem (5–8) and therefore hinder the solution of the inverse problem.

Algorithm 2 Algorithm for solving the forward problem (5–8). The same symbols are used to refer to quantities in (14–19) as well as their numerical approximations. For example, $\mathbf{A}$ refers to the differential operator as well as its matrix approximation.

1: Require: A target flip rate $F(x)$, velocity $v > 0$, an integer N, a starting position $-L/2 < x_0 < L/2$ and a discretization of the interval $[-L/2, L/2]$, $\{\chi_0, \chi_1, \ldots, \chi_n\}$.

2: Discretize the differential operators $\mathbf{A}$ and the adjoint $\mathbf{A}^*$ where

$$\mathbf{A} \begin{pmatrix} u_1 \\ u_2 \end{pmatrix} = \left\{ \begin{bmatrix} v\dfrac{\mathrm{d}}{\mathrm{d}x} & 0 \\ 0 & -v\dfrac{\mathrm{d}}{\mathrm{d}x} \end{bmatrix} + F(x) \begin{bmatrix} -1 & 1 \\ 1 & -1 \end{bmatrix} \right\} \begin{pmatrix} u_1(x) \\ u_2(x) \end{pmatrix},$$

$$\mathbf{A}^* \begin{pmatrix} p_1 \\ p_2 \end{pmatrix} = \left\{ \begin{bmatrix} -v\dfrac{\mathrm{d}}{\mathrm{d}x} & 0 \\ 0 & v\dfrac{\mathrm{d}}{\mathrm{d}x} \end{bmatrix} + F(x) \begin{bmatrix} -1 & 1 \\ 1 & -1 \end{bmatrix} \right\} \begin{pmatrix} p_1(x) \\ p_2(x) \end{pmatrix}.$$

Note that $\mathbf{A}$ must account for the boundary conditions $u_1(L/2) = 0$ and $u_2(-L/2) = 0$ respectively and $\mathbf{A}^*$ must account for the adjoint boundary conditions $p_1(-L/2) = 0$ and $p_2(L/2) = 0$.

3: Compute $s_1, \ldots, s_N$, the first N complex eigenvalues of $\mathbf{A}$ with smallest absolute value.

4: Compute the corresponding N eigenvectors of $\mathbf{u}_1, \ldots, \mathbf{u}_N$ of $\mathbf{A}$ and $\mathbf{p}_1, \ldots, \mathbf{p}_N$ of $\mathbf{A}^*$.

5: Compute the inner products $D_m = \int_{-L/2}^{L/2} \mathbf{p}_m^*(x) \mathbf{u}_m(x) \, \mathrm{d}x$ for $m = 1, \ldots, N$.

6: Compute the functions $h_m^{(1)}(t)$ and $h_m^{(2)}(t)$ in (15) and (16) for $m = 1, \ldots, N$.

7: Compute $a_1(x)$ and $a_2(x)$ in (17) and (18).

8: Compute

$$\mathbf{Z}(x_0, t) = -\sum_{m=1}^{N} \frac{\mathbf{u}_m(x_0)}{s_m D_m} [h_m^{(1)}(t) + h_m^{(2)}(t)], \tag{21}$$

as the N-term approximation to (14). If x_0 does not coincide with a grid point χ_j, use interpolation to find $\mathbf{u}_m(x_0)$.

9: Compute $W_1(x_0, t)$ and $W_2(x_0, t)$ by adding discontinuities of strength $a_1(x_0)$ and $a_2(x_0)$ at $t = -x_0/v + L/(2v)$ and $t = x_0/v + L/(2v)$ respectively to Z_1 and Z_2: see (12) and (13).

10: Output $W_1(x_0, t)$ and $W_2(x_0, t)$.

Proof of Theorem 1. Upon substituting (12) and (13) into (5) and (6), we find that $Z_{1,2}(x, t)$ satisfy

$$\frac{\partial Z_1}{\partial t} - v\frac{\partial Z_1}{\partial x} - F(x)(Z_2 - Z_1) = a_2(x)F(x)H[t - x/v - L/(2v)], \tag{22}$$

$$\frac{\partial Z_2}{\partial t} + v\frac{\partial Z_2}{\partial x} - F(x)(Z_1 - Z_2) = a_1(x)F(x)H[t + x/v - L/(2v)], \tag{23}$$

subject to the *homogeneous* boundary conditions $Z_1(L/2, t) = 0$, $Z_2(-L/2, t) = 0$ and initial conditions $Z_1(x, 0) = 0$, $Z_2(x, 0) = 0$ and $a_{1,2}$ are defined by (17) and (18). We now find a series representation for $Z_{1,2}(x, t)$. After taking Laplace transforms of (22) and (23), we find that $\tilde{\mathbf{Z}}(x, s) = [\tilde{Z}_1(x, s), \tilde{Z}_2(x, s)]^\mathsf{T}$ satisfies

$$(\mathbf{A} - s\mathbf{I})\tilde{\mathbf{Z}}(x, s) = -\frac{\tilde{\mathbf{N}}(x, s)}{s}, \tag{24}$$

$$\tilde{\mathbf{N}}(x,s) = F(x) \begin{bmatrix} a_2(x)\,\mathrm{e}^{-(L/(2v)+x/v)s} \\ a_1(x)\,\mathrm{e}^{-(L/(2v)-x/v)s} \end{bmatrix},$$

with boundary conditions $\tilde{Z}_1(L/2,s) = 0$, $\tilde{Z}_2(-L/2,s) = 0$. Equation (24) has a solution of the form

$$\tilde{\mathbf{Z}}(x,s) = \sum_{n=1}^{\infty} \frac{c_n(s)\mathbf{u}_n(x)}{s - s_n}, \tag{25}$$

where the vector eigenfunctions $\mathbf{u}_n(x) \in \mathbb{C}^2$ satisfy $\mathbf{A}\mathbf{u}_n = s_n\mathbf{u}_n$ for eigenvalues $s_n \in \mathbb{C}$. As an aside, when $F(x) = F_0$ is a constant, one can show that the eigenfunctions are proportional to $[-(\alpha^2 + \lambda_n^2)^{1/2}\sinh\lambda_n(x+\frac{1}{2}) + \lambda_n\cosh\lambda_n(x+\frac{1}{2}), \alpha\sinh\lambda_n(x+\frac{1}{2})]^{\mathrm{T}}$ with $\alpha \equiv F_0L/v$, the $\lambda_n \in \mathbb{C}$ satisfy the transcendental equation $-(\alpha^2 + \lambda_n^2)^{1/2}\tanh\lambda_n + \lambda_n = 0$ and the eigenvalues are given by $s_n = -\alpha - (\alpha^2 + \lambda_n^2)^{1/2}$.

Recall that if $\{\mathbf{u}_n\}$ are the eigenfunctions of $\mathbf{A}$ and $\{\mathbf{p}_m\}$ are the eigenfunctions of the adjoint operator $\mathbf{A}^*$, then $\langle \mathbf{p}_m, \mathbf{u}_n \rangle = 0$ unless $m = n$. Substituting (25) into (24), left-multiplying both sides of by $\mathbf{p}_m^*$ and integrating, we find that

$$c_n(s) = \frac{\langle \mathbf{p}_m(x), \tilde{\mathbf{N}}(x,s) \rangle}{sD_m},$$

where D_m is defined by (19). (One cannot obtain c_n by invoking orthogonality of $\{\mathbf{u}_n\}$ since $\mathbf{A}$ is not self-adjoint.) We now take the inverse Laplace transform of (25) and switch the order of integration to obtain the continuous parts of the CDFs:

$$\mathbf{Z}(x,t) = \sum_{m=1}^{\infty} \frac{\mathbf{u}_m(x)}{D_m} \left\{ \int_{-L/2}^{L/2} \mathrm{d}y\, p_m^{(1)*}(y)a_2(y)F(y) \int_{\gamma-\mathrm{i}\infty}^{\gamma+\mathrm{i}\infty} \frac{\mathrm{d}s}{2\pi\mathrm{i}} \frac{\mathrm{e}^{(t-y/v-L/(2v))s}}{s(s-s_m)} \right.$$

$$\left. + \int_{-L/2}^{L/2} \mathrm{d}y\, p_m^{(2)*}(y)a_1(y)F(y) \int_{\gamma-\mathrm{i}\infty}^{\gamma+\mathrm{i}\infty} \frac{\mathrm{d}s}{2\pi\mathrm{i}} \frac{\mathrm{e}^{(t+y/v-L/(2v))s}}{s(s-s_m)} \right\}, \quad \mathrm{Re}\,\gamma > 0,$$

$$= -\sum_{m=1}^{\infty} \frac{\mathbf{u}_m(x)}{s_mD_m}[h_m^{(1)}(t) + h_m^{(2)}(t)],$$

where $h_m^{(1)}(t)$ and $h_m^{(2)}(t)$ are given by (15) and (16), respectively.   □

2.2 *Monte Carlo simulation using Rejection–Acceptance*

We now give details of our Monte Carlo method (Algorithm 3). This method can be used to simulate a Broadwell particle with spatially dependent velocity, even though for our inverse problem, the particles always have constant velocity. The method is based on the Rejection–Acceptance method (Asmussen & Glynn, 2010), a common method for drawing random variables from a PDF whose functional form is known, but non-standard. We note four important points about the algorithm.

(1) The algorithm samples from $w_1(y_0,t)$ or $w_2(y_0,t)$ depending on the initial velocity; see (28).

(2) The algorithm generates random variables for the time periods in between the state transitions θ (the 'flip times'). For a Broadwell process with a constant transition rate, the flip times are exponentially distributed. For a *spatially dependent* transition rate $F(y)$, the flip time $\theta \equiv t_{j+1} - t_j$

is distributed according to

$$\theta \sim Q(t) \equiv F[y(t)] \exp[-p(t)],$$

$$p(t) = \int_0^t F[y(t')] \, dt',$$

(26)

where the position of the particle satisfies $dy(t)/dt = v(y)$. We sample from $Q(t)$ using a Rejection–Acceptance method (Asmussen & Glynn, 2010): suppose that there exist constants F_{min} and F_{max} satisfying $0 < F_{min} \leqslant F(y) \leqslant F_{max} < \infty$ for $-L/2 < y < L/2$. Then

$$Q(t) \leqslant C F_{min} \exp(-F_{min}t) \equiv P(t),$$

where $C = F_{max}/F_{min}$ and so an exponential distribution can be used as an envelope function.

Algorithm 3 Generating exit times from a Broadwell process.

1: Require: an interval size L, a starting position $-L/2 \leqslant y_0 \leqslant L/2$, functions $F(y), v(y) \in C(-\infty,$
  $+\infty)$, $F_{min}, F_{max} > 0$ where $F_{min} \leqslant F(y) \leqslant F_{max}$ for $y \in [-L/2, L/2]$.
2: Let $P(t) \equiv F_{max} \exp(-F_{min}t)$.
3: Set $j = 0$ and $t_j = 0$.
4: **while** $-L/2 < y_j < L/2$ **do**
5:   Draw $\theta \sim \exp(F_{min})$
6:   Compute $p(\theta)$ and $y(\theta)$ by numerically solving

$$\frac{dp(t)}{dt} = F(y),$$

(27)

$$\frac{dy(t)}{dt} = \begin{cases} (-1)^j v(y), & \{\text{for positive velocity at } t = 0\} \\ (-1)^{j+1} v(y), & \{\text{for negative velocity at } t = 0\} \end{cases}$$

(28)

  on $t \in [0, \theta]$, subject to initial conditions $p(0) = 0$ and $y(0) = y_j$.
7:   Set $Q(\theta) = F[y(\theta)] \exp[-p(\theta)]$
8:   Draw $\rho \sim U(0, 1)$
9:   **if** $\rho < Q(\theta)/P(\theta)$ **then**
10:     $j \leftarrow j + 1$ {acceptance}
11:     Set $y_j = y(\theta)$ and $t_j = t_{j-1} + \theta$
12:     Goto 4
13:   **else**
14:     Goto 5 {rejection}
15:   **end if**
16: **end while**{Particle has left interval}
17: **if** $y_j > L/2$ **then**
18:   Output the exit time as $t_j + \int_{y_j}^{L/2} v^{-1}(y) \, dy$.
19: **else**
20:   Output the exit time as $t_j + \int_{y_j}^{-L/2} (-v^{-1}(y)) \, dy$.
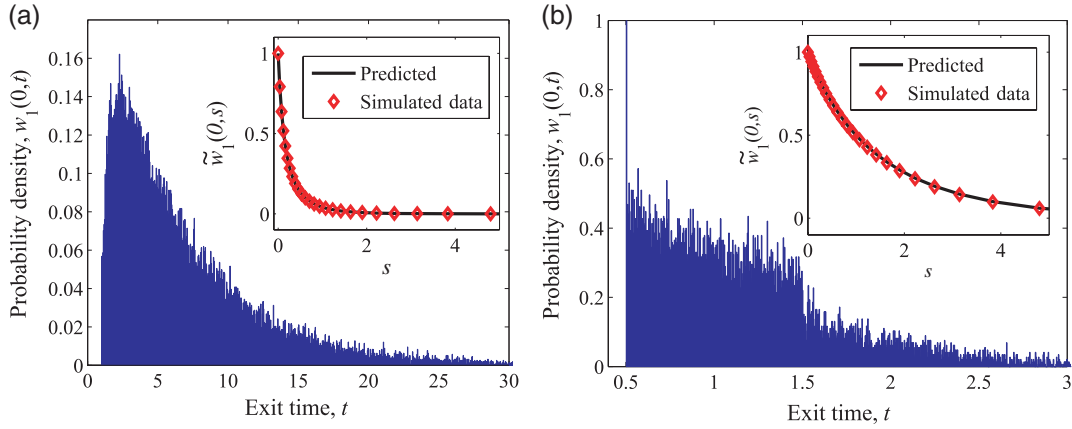21: **end if**

FIG. 2. Simulated exit times of a Broadwell process. Although probability densities are shown here, CDFs are used to infer the flip rate function. (a) $F(x) = 10x^3 + 5e^x + 1$, $v = \frac{1}{2}$, (b) $F(x) = 1 + x^2$, $v = 1$. Insets show Laplace-transformed data. Solid line: solution to (9) and (10). Diamonds: Laplace transform of histogram data. The number of realizations was $N = 40,000$ in each case.

(3) Once the flip time θ is generated, the flip position y_{j+1} can be found by solving $\int_{y_j}^{y_{j+1}} v^{-1}(y)\,dy = \theta$. This integral could be expensive to calculate if it has to be done many times. Also, every evaluation of $Q(t)$ requires computing the integral $p(t)$ in (26). Both of these issues are handled simultaneously in our algorithm through the solution of the pair of ordinary differential equations (27) and (28). For the special case where v is a constant, (27) and (28) should be replaced with $dp/dt = F(y_j \pm vt)$ and $y(t) = y_j \pm vt$.

(4) When solving the differential equations (27) and (28), F may have to be evaluated outside of the interval $[-L/2, L/2]$. Because the form of $F(y)$ outside $[-L/2, L/2]$ does not affect the exit time, we simply take $F(y) = F(L/2)$ for $y > L/2$ and $F(y) = F(-L/2)$ for $y < -L/2$.

Figure 2 shows the PDFs $w_1(0, t)$ generated by the algorithm for two different $F(x)$ when $v(x) =$ constant. By definition, w_1 is the exit time density for a particle that initially has velocity $v > 0$. Therefore, the solution $w_1(x, t)$ in (1) contains delta functions that correspond to an immediate particle exit at a time $t_c \equiv (L/2 - x)/v$. The reason is if t is the particle exit time and θ is the time before the *first* state transition, then

$$P(t = t_c) = P(\theta \geqslant t_c) = \int_{t_c}^{\infty} Q(t')\,dt' > 0. \tag{29}$$

Hence, the probability distribution of the exit times will always contain point masses (delta functions) of probability located at $t = t_c$ (Masoliver & Weiss, 1994). In Fig. 2(b), a numerical approximation of this delta function can be seen. The height of this 'spike' is controlled by the size of the bins used when creating the histogram and becomes unbounded as the bin size tends to zero and the number of trials tends to infinity. These delta distributions are always present in the exact solution but they may not always be visible in the numerical solution if the number of trials is small or the bin size is large; see Fig. 2(a), for example.

2.2.1 *Generation of noisy distributions from a finite number of exit times*   We always use Algorithm 3 to generate two sets of N exit times $\{\tau_j^{(1)}\}$ and $\{\tau_j^{(2)}\}$. With this notation, $\tau_j^{(i)}$ ($1 \leqslant j \leqslant N$, $i = 1, 2$) is the jth exit time conditioned on the particle having initial velocity $(-1)^{i+1}v$. Assuming that $\{\tau_j^{(1)}\}$ and $\{\tau_j^{(2)}\}$ are sorted in ascending order, noisy cumulative densities $W_{1,\text{data}}(t)$ and $W_{2,\text{data}}(t)$ are computed as

$$W_{i,\text{data}}(t) = \begin{cases} 0 & \text{if } t < \tau_1^{(i)}, \\ \dfrac{m}{N} & \text{if } \tau_1^{(i)} < t < \tau_N^{(i)}, \\ 1 & \text{if } t \geqslant \tau_N^{(i)}, \end{cases} \tag{30}$$

where m is the unique index satisfying $\tau_m^{(i)} < t < \tau_{m+1}^{(i)}$.

The noisy Laplace transform of a finite number of exit times is calculated through

$$\tilde{w}_{j,\text{data}}(s) = \begin{cases} \displaystyle\int_0^\infty e^{-st} \frac{dW_{j,\text{data}}(t)}{dt}\, dt = s\tilde{W}_{j,\text{data}}(s), & s > 0, \\ 1, & s = 0, \end{cases} \tag{31}$$

where

$$\tilde{W}_{j,\text{data}}(s) = \int_0^\infty e^{-st} W_{j,\text{data}}(t)\, dt = \int_0^1 e^{-st[\eta]} W_{j,\text{data}}(t[\eta]) \frac{d\eta}{(1-\eta)^2}, \tag{32}$$

where $j = 1, 2$ and $t[\eta] = \eta/(1 - \eta)$. We avoid 'binning' when calculating $\tilde{w}_{j,\text{data}}$, since this introduces a corresponding discretization error. The integral in (32) can be calculated using the trapezium rule on equally spaced abscissae in η.

2.3 *Projection method to solve inverse problem*

We now briefly describe our algorithms for reconstructing the flip rate function $F(x)$ from the two distributions of exit times $w_{1,\text{data}}(t)$ and $w_{2,\text{data}}(t)$. These distributions can come from simulating the Broadwell process directly through Algorithm 3 or through a one-time solution of the forward problems (9–11) or (5–8). We implement two related algorithms. The first method uses the exit time data directly (t-method) and the second method uses Laplace-transformed exit time data (s-method). Pseudocode for the two methods is given in Algorithms 4 and 5.

In both methods, we represent the trial flip rate function $F_M(x)$ and the target flip rate function $F^*(x)$ as a linear combination of Legendre polynomials on $[-L/2, L/2]$:

$$F_M(x) = \sum_{j=0}^{M-1} a_j \phi_j(x). \tag{33}$$

For example, $\phi_0(x) = 1$, $\phi_1(x) = 2x/L$, $\phi_2(x) = 6(x/L)^2 - \frac{1}{2}$.

Algorithm 4 Reconstruction of flip rate coefficients using the *t*-method.

1: Require: An integer M, an interval length L, target flip rate function $F^*(x)$, a particle speed $v > 0$, a starting position $-L/2 < x_0 < L/2$ and the first M legendre polynomials on $(-L/2, L/2)$, $\phi_1, \ldots, \phi_M$ (see text for details).

2: Generate noisy cdfs of the exit time $W_{1,\text{data}}(x_0, t)$ and $W_{2,\text{data}}(x_0, t)$ for $F^*(x)$ using Algorithm 3.

3: For a given $\mathbf{a} = (a_0, a_1, \ldots, a_{M-1}) \in \mathbb{R}^M$, define $F_M(x) = \sum_{j=0}^{M-1} a_j \phi_j(x)$. Let $W_{1,2}(x_0, t; \mathbf{a})$ be the solution to the forward problem (5–8) with $F = F_M$, calculated using Algorithm 2.

4: Find $\mathbf{a} = \hat{\mathbf{a}}$ that minimizes

$$\Pi_1(\mathbf{a}) = \int_0^{L/v} |W_1(x_0, t; \mathbf{a}) - W_{1,\text{data}}(x_0, t)|^2 \, \mathrm{d}t + \int_0^{L/v} |W_2(x_0, t; \mathbf{a}) - W_{2,\text{data}}(x_0, t)|^2 \, \mathrm{d}t. \quad (34)$$

Integrating through discontinuities can be avoided by noting that $W_{1,2}(x, t) = 0$ when $t < \min(L/(2v) - x/v, x/v + L/(2v))$. The lower limits of integration in (34) can be replaced with $(L/(2v) - x_0/v)^+$ when $0 \leqslant x_0 < L/2$ and $(x_0/v + L/(2v))^+$ when $-L/2 < x_0 \leqslant 0$.

5: Output $\hat{F}(x) \equiv \sum_{j=0}^{M-1} \hat{a}_j \phi_j(x)$ as the estimate of the flip rate function for the exit time distributions $W_{1,\text{data}}(x_0, t)$ and $W_{2,\text{data}}(x_0, t)$.

Algorithm 5 Reconstruction of flip rate coefficients using the *s*-method.

1: Require: An integer M, an interval length L, a target flip rate function $F^*(x)$, a particle speed $v > 0$, a starting position $-L/2 < x_0 < L/2$ and the first M Legendre polynomial on $(-L/2, L/2)$, $\phi_1, \ldots, \phi_M$ (see text for details).

2: Use $F^*(x)$ to generate Laplace-transformed exit time pdfs $\tilde{w}_{1,\text{data}}(x_0, s)$ and $\tilde{w}_{2,\text{data}}(x_0, s)$ through Algorithm 3.

3: For a given $\mathbf{a} \in \mathbb{R}^M$, let $\tilde{w}_{1,2}(x_0, s; \mathbf{a})$ be the solution to the forward problem (9–11) calculated using Algorithm 1 with flip rate function defined by $\mathbf{a} = \{a_0, a_2, \ldots, a_{M-1}\}$:

$$F_M(x) = \sum_{j=0}^{M-1} a_j \phi_j(x).$$

4: Find $\mathbf{a} = \hat{\mathbf{a}}$ that minimizes

$$\Pi_2(\mathbf{a}) = \int_0^\infty |\tilde{w}_1(x_0, s; \mathbf{a}) - \tilde{w}_{1,\text{data}}(x_0, s)|^2 \, \mathrm{d}s + \int_0^\infty |\tilde{w}_2(x_0, s; \mathbf{a}) - \tilde{w}_{2,\text{data}}(x_0, s)|^2 \, \mathrm{d}s. \quad (35)$$

The integral in (35) is calculated using a change of variable $s[\xi] = \xi/(1 - \xi)$ so that

$$\Pi_2 = \sum_{j=1}^2 \int_0^1 [\tilde{w}_j(x_0, s[\xi], \mathbf{a}) - \tilde{w}_{j,\text{data}}(x_0, s[\xi])]^2 \frac{\mathrm{d}\xi}{(1 - \xi)^2},$$

which can be computed using the trapezium rule on equally spaced abscissae on [0,1].

5: Output $\hat{F}(x) \equiv \sum_{j=0}^{M-1} \hat{a}_j \phi_j(x)$ as the estimate of the flip rate function for the exit time distributions $\tilde{w}_1(x_0, s)$ and $\tilde{w}_2(x_0, s)$.

Our aim is to find coefficients $a_1, \ldots, a_M$ to minimize the objective functions for the t-method and s-methods, Π_1 and Π_2, respectively. These take the form

$$\Pi_1(\mathbf{a}) = \int_0^{L/v} |W_1(x_0, t; \mathbf{a}) - W_{1,\mathrm{data}}(x_0, t)|^2 \, \mathrm{d}t + \int_0^{L/v} |W_2(x_0, t; \mathbf{a}) - W_{2,\mathrm{data}}(x_0, t)|^2 \, \mathrm{d}t,$$

$$\Pi_2(\mathbf{a}) = \int_0^\infty |\tilde{w}_1(x_0, s; \mathbf{a}) - \tilde{w}_{1,\mathrm{data}}(x_0, s)|^2 \, \mathrm{d}s + \int_0^\infty |\tilde{w}_2(x_0, s; \mathbf{a}) - \tilde{w}_{2,\mathrm{data}}(x_0, s)|^2 \, \mathrm{d}s.$$

The data sets $W_{j,\mathrm{data}}(x_0, t)$ and $\tilde{w}_{j,\mathrm{data}}(x_0, s)$ associated with $F^*(x)$ can be computed from individual exit times using (30) and (31), respectively.

Minimization of Π_1 and Π_2 with respect to $\mathbf{a}$ was performed using Matlab routines `fminunc.m` and `lsqnonlin.m` for the t and s methods, respectively, with tolerances `TolFun` and `TolX` set to 10^{-14}. The initial guess for the coefficients was always $a_j = 1$ for $j = 0, 1, \ldots, M - 1$, unless otherwise stated. The minimizing coefficients $\hat{a}_j$ then define the reconstructed flip rate through $\hat{F}(x) = \sum_{j=0}^{M-1} \hat{a}_j \phi_j(x)$.

An obvious limitation of the projection method is that the method does not converge for non-polynomial F^* and polynomial F^* with degree $> M$. However, as we shall see in Section 3, the method may still be used to find reasonable approximations in these cases.

3. Results and discussion

3.1 *Flip rate reconstruction*

We used the projection algorithm discussed in Section 2.3 to reconstruct flip rate functions from data generated using Monte Carlo simulation (see Section 2.2). In the following discussion, let N be the number of exit times for each initial velocity $+v$, $-v$, so that the total number of exit times is always $2N$. We also take the starting position $x_0 = 0$, interval length $L = 1$ and particle speed $v = 1$ unless otherwise stated.

For Fig. 3, we reconstruct some 'structurally simple' smooth functions that have few extrema within $(-L/2, L/2)$ and find that the accuracy of the reconstructions improves as the noise in the data decreases. For the '$N = \infty$' cases, artificial, noiseless data are generated by solving the forward problems (5–8) and (9–11) with $F = F^*$. Panels (a–f) indicate that, for a given N, the t-method generally outperforms the s-method since the associated errors are smaller. In (a, b), we reconstruct a cubic polynomial by recovering $M = 4$ Legendre coefficients. In (c, d), we attempt to reconstruct a transcendental function by representing $F^*(x)$ with $M = 5$ coefficients. Although $\|F_M - F^*\|_\infty \nrightarrow 0$ as the noise decreases, we are still able to find a reasonable approximation F_M so that $\|F_M - F^*\|_\infty$ is not too large. The s-method converges to the correct solution for perfect data but the inclusion of a small amount of noise renders the method unstable, resulting in a large error. This kind of behaviour also occurs with the t-method when $M \gtrsim 5$ and is typical in many ill-posed problems (see below). In (e) and (f), we reconstruct flip rate functions from a relatively small number of exit times by taking $M = 3$ basis functions; however, a smaller M restricts the range of admissible target functions.

If we have no *a priori* knowledge on $F^*(x)$ (e.g. it may be a high-degree polynomial, have many extrema or be discontinuous), our method may not capture $F^*(x)$ accurately. For our method to be successful, it is important that we know beforehand that $F^*(x)$ is smooth and structurally not too complex.
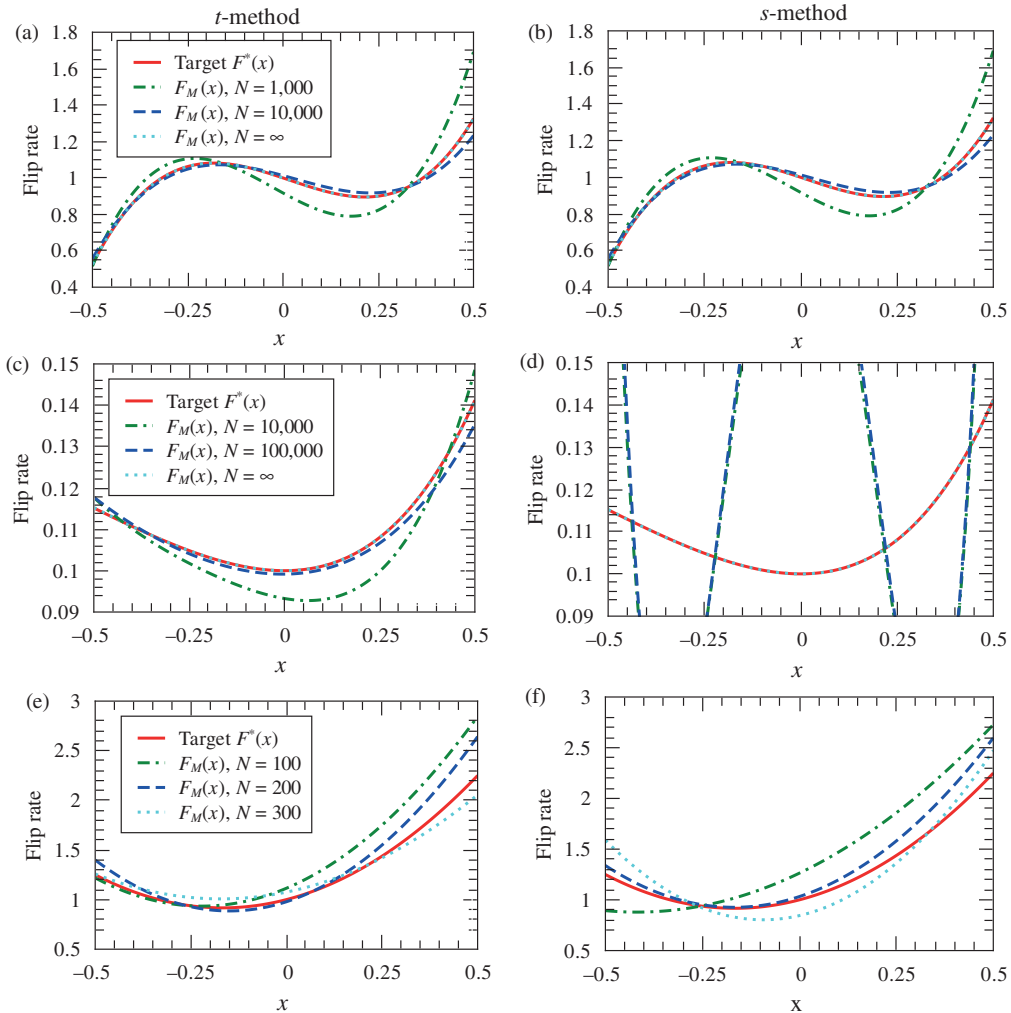
Fig. 3. Reconstructed approximations to flip rate functions $F^*(x)$ from noisy exit time data. (a, b) $F^*(x) = 1 - 0.7x - 0.3x^2 + 6x^3$, $M = 4$; (c, d) $F^*(x) = x^2 e^{-x}/10 + 1/10$, $M = 5$; (e, f) $F^*(x) = 1 + x + 3x^2$, $M = 3$. The *t*-method was used in the left panels and the *s*-method was used in the right panels. $N = \infty$ corresponds to perfect, noiseless data, which is generated by solving the forward problems (5–8) and (9–11).

Increasing the number of basis functions M increases the range of functions we can accurately represent. Provided F^* is smooth enough, it can always be represented through its Taylor series and our method strives to capture its first M coefficients. Ideally, we would like M to be as large as possible to represent any $F^*(x) \in C^\infty(-L/2, L/2)$. However, in practice it is difficult to reliably reconstruct $F^*(x)$ (even polynomials) when $M \gtrsim 5$. The reason, which is common to all projection methods (Fok & Chou, 2010; Kress, 1989), is that as the finite-dimensional approximation to $F^*(x)$ improves with $M \to \infty$, the method becomes more unstable due to ill-posedness. In this limit, minimizing the objective functions (34) and (35) is prone to large errors.

TABLE 1 *Local condition numbers κ_s and κ_t for $F^*(x) = 1 + x$ corresponding to the objective functions* (35) *and* (34), *respectively*; M *denotes the number of basis functions used in* (33)

M	κ_t	κ_s
2	5.3×10^2	3.1×10^2
3	1.0×10^4	3.3×10^4
4	1.4×10^5	3.5×10^6
5	1.0×10^6	1.6×10^8

TABLE 2 *Local condition numbers for $F^*(x) = 1 - x + x^2$; see Table* 1 *for details*

M	κ_t	κ_s
3	5.0×10^5	1.8×10^5
4	3.5×10^6	1.6×10^7
5	6.7×10^6	5.2×10^8

3.2 *Instability of the projection method*

Numerically, the instability discussed above may be quantified by examining the condition number of the objective function near its minimum. Specifically, we study the Hessian (matrix of second partial derivatives) of the objective functions Π_1 and Π_2 in (34) and (35) with respect to the coefficients a_j, $j = 0, \ldots, M - 1$:

$$H_{ij}^{(1)} \equiv \frac{\partial^2 \Pi_1}{\partial a_i \partial a_j}\bigg|_{a_i = a_i^*, a_j = a_j^*}, \quad H_{ij}^{(2)} \equiv \frac{\partial^2 \Pi_2}{\partial a_i \partial a_j}\bigg|_{a_i = a_i^*, a_j = a_j^*}, \tag{36}$$

for $i, j = 0, \ldots, M - 1$. In (36), a_i^* are the target coefficients of a polynomial flip rate function: $F^*(x) = \sum_{i=0}^{M-1} a_i^* \phi_i(x)$. The condition number of a matrix A is defined as the ratio of its largest eigenvalue to its smallest: $\kappa = \lambda_{\max}(A)/\lambda_{\min}(A)$. Since the eigenvalues represent the principle curvatures of $\Pi_{1,2}$ at the point $\mathbf{a}^*$, they are always positive; a very large condition number indicates that Π_1 or Π_2 is locally very flat at $\mathbf{a} = \mathbf{a}^*$ and finding $\mathbf{a}^*$ numerically is prone to errors. On the other hand, a moderate-sized condition number indicates only a small difference in curvatures near $\mathbf{a}^*$ and so finding the minimum numerically should not be difficult. Tables 1 and 2 show that both condition numbers for the *t*- and *s*-methods grow exponentially as the number of basis functions M increases. For $M = 5$ basis functions, the condition numbers for the *t*-method are consistently two orders of magnitude smaller than those for the *s*-method. This suggests that fitting to the exit time data directly (as opposed to its Laplace transform) leads to more effective algorithms and better estimates for the flip rate function. This is confirmed in our numerical experiments since occasionally the *t*-method is able to recover $M = 5$ coefficients of a quartic polynomial $F(x)$, but the *s*-method is seldom able to do so.

3.3 *Sensitivity of reconstruction to advection speed*

We also explore the accuracy of our reconstruction for different advection speeds v, given a fixed number of exit times when $F^*(x)$ is a polynomial of degree $\leqslant M - 1$. In Fig. 4, we see that, for both methods, when the velocity is either much less or much larger than unity, the associated error is large. (Although the upper limit of the objective function (34) depends on the value of v used, we checked that the non-monotonic behaviour in $\|F_M - F^*\|_\infty$ was not sensitive to the upper limit of integration.)
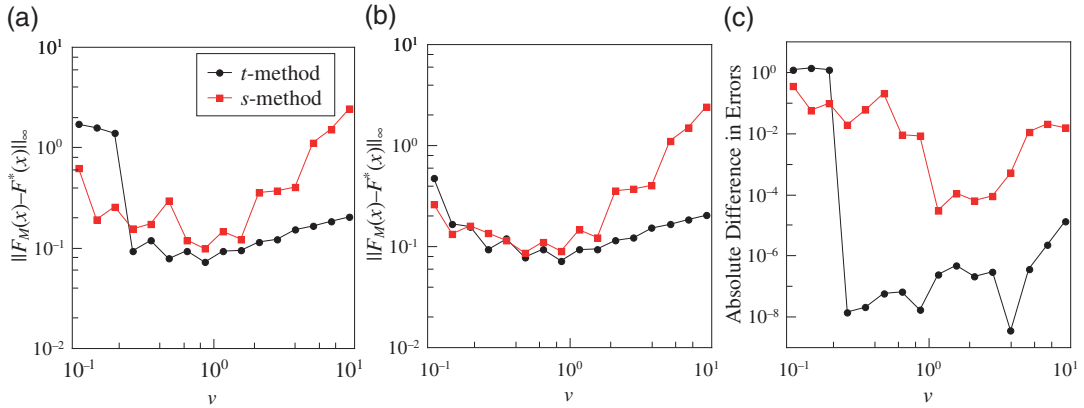
FIG. 4. Error in the reconstructed flip rate as a function of particle velocity. Each point is an average over 10 sets of $2N = 20,000$ exit times. Target flip rate $F^*(x) = \frac{9}{4}x^2 - \frac{3}{4}x + \frac{9}{16}$, corresponding to target coefficients $\mathbf{a}^* = [0.75, -0.375, 0.375, 0]$. Initial guesses are (a) $\mathbf{a} = [1, 1, 1, 1]$, (b) $\mathbf{a} = [0.76, -0.385, 0.365, 0.01]$. The same exit times were used for both (a) and (b). The difference in the errors is shown in (c).

In practice, there are always two sources of error in the reconstruction of F^*: the first is from noise in the data and the second stems from the minimization procedure itself:

$$\text{Total error} = \text{error from noise in data} + \text{error from minimization.} \tag{37}$$

If the minimization of the objective functions (34) or (35) was achieved with zero error, noisy exit times would still produce an error in the reconstructed F. On the other hand, for noiseless data, the flat minima and large condition numbers discussed above would produce an erroneous F from the minimization. It is hard to separate the two types of error in (37), but some insight can be gained by comparing Fig. 4(a,b) which differ only in the starting values for the coefficients $a_0, \ldots, a_{M-1}$; in particular, the exit times for each value of v for each figure are identical. When we move the initial guess for the coefficients closer to their target values in (b), we greatly reduce the error in minimization since the accuracy of minimization algorithms depends on the quality of the initial guess. Therefore, the error in (b) comes mainly from *noise in the data*. Since the exit times were identical for (a) and (b), the difference of the errors in (a) and (b)—shown in (c)—represents the *error from minimization* which is associated with large condition numbers and flat extrema. We note that the error from minimization from the *s*-method is much larger than the corresponding error from the *t*-method for a wide range of v values.

When the dominant error stems from noise in the data (as is the case in Fig. 4(b)), we can understand why $v = \mathrm{O}(1)$ provides the most accurate reconstruction by analysing how well the Monte Carlo simulations approximate the moments of the exit time distribution. We prove the following theorem.

THEOREM 2 Let $T_1^{(n)}(x)$ and $T_2^{(n)}(x)$ be the nth moments of the exit time conditioned on the particle starting at position x with initial velocity $+v$ and $-v$, respectively. Then the moments have the asymptotic behaviour

$$T_{1,2}^{(k)}(x) = \begin{cases} O\left(\dfrac{k!}{v^{2k}}\right), & v \ll 1, \\[2mm] O\left(\dfrac{k!}{v^k}\right), & v \gg 1. \end{cases} \tag{38}$$

Proof. We have $T_{1,2}^{(n)}(x) = (-\partial/\partial s)^n \tilde{w}_{1,2}(x,s)|_{s=0}$ for $n \geqslant 0$, and from (9) and (10), these moments satisfy the coupled equations

$$-v\frac{dT_1^{(n)}}{dx} - F(x)(T_2^{(n)} - T_1^{(n)}) = nT_1^{(n-1)},$$

$$v\frac{dT_2^{(n)}}{dx} - F(x)(T_1^{(n)} - T_2^{(n)}) = nT_2^{(n-1)},$$

subject to the boundary conditions $T_1^{(n)}(L/2) = 0$ and $T_2^{(n)}(-L/2) = 0$ where $n \geqslant 1$ and $T_{1,2}^{(0)}(x) = 1$. After some algebra, we find expressions for the moments in terms of indefinite integrals:

$$T_1^{(n)}(x) = -\frac{n}{v^2}\int dx F(x) \int dx[T_1^{(n-1)}(x) + T_2^{(n-1)}(x)] - \frac{n}{v}\int dx T_1^{(n-1)}(x), \tag{39}$$

$$T_2^{(n)}(x) = -\frac{n}{v^2}\int dx F(x) \int dx[T_1^{(n-1)}(x) + T_2^{(n-1)}(x)] + \frac{n}{v}\int dx T_2^{(n-1)}(x). \tag{40}$$

When $v \ll 1$, we retain the first integral in each of (39) and (40) to find $T_{1,2}^{(k)} = O(k!/v^{2k})$. If $v \gg 1$, we retain the second integrals to find $T_{1,2}^{(k)} = O(k!/v^k)$. □

In (38), we see that the moments have a different asymptotic form depending on whether v is small or large. When $v \ll 1$, the random walker is in the diffusive limit where all the moments (except for the zeroth moment) diverge. On the other hand, when $v \gg 1$, the particle is in the ballistic limit: all moments except for the zeroth moment are asymptotically small and, to leading order, independent of $F(x)$.

Now consider approximating $w_1(x_0, t)$ or $w_2(x_0, t)$ with their noisy counterparts generated by the Monte Carlo simulations. How well are the $w_{1,2}(x_0, t)$ approximated? One way to quantify the accuracy is by calculating the error in the moments of the noisy distribution. Given an initial velocity $+v$, let $\{\tau_j\}, 1 \leqslant j \leqslant N$ be the N generated exit times (the following argument with initial velocity $-v$ is almost identical). Then, by the central limit theorem, the kth moment is approximately distributed according to

$$\frac{1}{N}\sum_{j=1}^N \tau_j^k \sim \mathcal{N}\left(T_1^{(k)}, \frac{\text{Var}(\tau_j^k)}{N}\right),$$

where $\mathcal{N}(\mu, v)$ is a normal distribution with mean μ and variance v. Therefore, a measure of the error incurred when calculating the kth sample moment is

$$N^{-1/2}\sqrt{\text{Var}(\tau_j^k)} = N^{-1/2}\sqrt{T_1^{(2k)} - T_1^{(k)2}} = \begin{cases} O(N^{-1/2}v^{-2k}), & v \ll 1, \\ O(N^{-1/2}v^{-k}), & v \gg 1, \end{cases} \tag{41}$$

using (38) and $\text{Var}(\tau_j^k) = E[(\tau_j^k - T_1^{(k)})^2]$. Therefore, from (41), a quick rule of thumb for the accuracy of the Monte Carlo generated exit time distribution is that the error scales as $N^{-1/2}$, where N is the number of trials.

It is evident from (41) that, for a fixed number of realizations, the error in the kth moment diverges as v^{-2k} as $v \to 0$ and the underlying exit time distribution is badly approximated in the limit of small v. On the other hand, as $v \to \infty$, although the error in the moments tends to zero, the moments themselves also tend to zero. From (29), the probability that a Broadwell particle with initial velocity $+v$ exits in
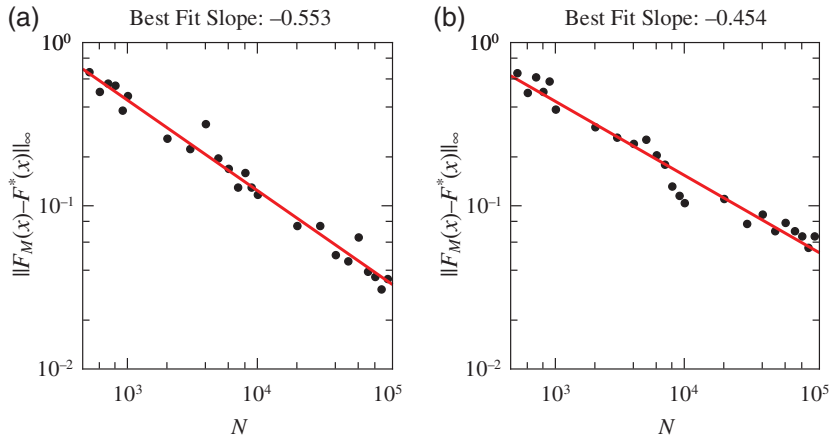
FIG. 5. Dependence of error in reconstructed flip rate function $F(x)$ on the number of exit times per initial state N when $F(x) = 1 - 0.7x - 0.3x^2 + 6x^3$ using the (a) t-method, (b) s-method. For each N, the error is calculated by performing minimizations for 10 data sets and taking the average, with each set containing $2N$ exit times.

time t_c tends to 1 as $v \to \infty$: for large v, the generated list of exit times is populated almost exclusively by t_c (and $t_c \to 0$ as $v \to \infty$). From a single exit time, it is very difficult to infer any information about $F(x)$. In both limiting cases, since the distribution of exit times is poorly captured by a finite number of realizations, the quality of the reconstruction suffers.

Finally, we systematically explore the effect of noise on the reconstruction quality. In Fig. 5, we plot the error of the reconstructed $F_M(x)$ against the number of exits. For a wide range of polynomials $F^*(x)$, using both the t- and s-methods, we find that the error in the reconstructed function scales as $O(N^{-1/2})$. In particular, we see that, for $N = O(10^4)$, the error $\|F_M - F^*\|_\infty = O(10^{-1})$, whereas N must exceed $O(10^6)$ for the error to fall below $O(10^{-2})$. These estimates are mean values: the accuracy resulting from fitting one data set to the next will always vary because the noise in each set is different.

4. Conclusions

In this paper, we made three contributions. The first is a pair of algorithms, Algorithms 4 and 5, that can be used to estimate the flip rate function of a 1D, constant-speed Broadwell process from the distribution of exit times out of a finite interval. In particular, the t-method is based on a novel series solution of the backward equation (5–8); see Theorem 1. The second is a simulation method, Algorithm 3, that is, used in this paper to generate the exit times of a Broadwell particle. The algorithm can accommodate spatially dependent flip rates and velocities. Our final contribution is a set of calculations and asymptotic results that quantify the errors in approximating the exit time distribution with simulated data, and the corresponding error in the flip rate reconstruction.

We found that polynomial transition rates could be reconstructed if the degree of the polynomial was not too large ($\lesssim 4$) and that fitting to the exit time distribution (t-method) directly versus fitting to the Laplace-transformed distribution (s-method) generally allowed the reconstruction of one extra coefficient in the representation of $F(x)$. Providing our initial guess for the coefficients of $F(x)$ was not too far from the target coefficients, we were able to find $F(x)$ to within $O(10^{-1})$ using $O(10^4)$ exit times. We were also able to find good approximations to non-polynomial flip-rate functions, provided they are

smooth and slowly varying. Finally, we experimented with reconstructions using different advection speeds. We found that $v = O(1)$ yielded the most accurate reconstructions because very small or large values of v in the Monte Carlo simulations gave poor representations of the true underlying exit time distribution.

Our results suggest that the t-method is an effective method to infer the spatially dependent flip rate function of a two-state Broadwell process, if it is known *a priori* that this function is smooth and structurally simple. The t-method involves explicitly solving for the CDFs (5–8), tracking the discontinuities via (12–13) and minimizing the objective function (34). With this method, one can often find $M = 4$ coefficients from about $2N = 20,000$ exit times. The s-method usually reconstructs one less coefficient than the t-method for the same number of exit times, and is more sensitive to the initial guess. However, it is much simpler to implement and only involves solving the ordinary differential equations (9–11) and minimizing (35).

We see two main extensions to this work. The first is to reconstruct spatially dependent advection velocities $v(x)$ as well as transition rates $F(x)$. The second is to develop alternative algorithms for reconstruction. We showed in this paper that as the number of coefficients representing the flip rate function increases, our method becomes unstable due to the presence of flat minima in the objective functions (see (34) and (35) and Tables 1 and 2). This instability could be alleviated by introducing a small regularization parameter in the objective functions (34) and (35) or developing iterative algorithms based directly on (1–4) and (5–8).

Acknowledgements

Funding

References

ARRIDGE, S. R. (1999) Optical tomography in medical imaging. *Inverse Probl.*, **41**, 41–93.

ARRIDGE, S. R. & HEBDEN, J. C. (1997) Optical imaging in medicine: II. Modelling and reconstruction. *Phys. Med. Biol.*, **42**, 841–853.

ASMUSSEN, S. & GLYNN, P. W. (2010) *Stochastic Simulation: Algorithms and Analysis*. Berlin: Springer.

BAL, G. & CHOU, T. (2003) On the reconstruction of diffusions from first-exit time distributions. *Inverse Probl.*, **20**, 1053–1065.

BICOUT, D. J. (1997) Green's functions and first passage time distributions for dynamic instability of microtubules. *Phys. Rev. E*, **56**, 6656–6667.

BROADWELL, J. E. (1964a) Shock structure in a simple discrete velocity gas. *Phys. Fluids*, **7**, 1243.

BROADWELL, J. E. (1964b) Study of rarefied shear flow by the discrete velocity method. *J. Fluid Mech.*, **19**, 401.

CHRISTLIEB, A. J., ROSSMANITH, J. A. & SMEREKA, P. (2004) The Broadwell model in a thin channel. *Commun. Math. Sci.*, **2**, 443–476.

DE HOOP, M. V., SMITH, H., UHLMANN, G. & VAN DER HILST, R. D. (2009) Seismic imaging with the generalized radon transform: a curvelet transform perspective. *Inverse Probl.*, **25**, 025005.

DUDKO, O. K. (2009) Single-molecule mechanics: new insights from the escape-over-a-barrier problem. *Proc. Natl Acad. Sci. USA*, **106**, 8795–8796.

Fok, P.-W., Guo, C.-L., & Chou, T. (2008) Charge-transport-mediated recruitment of DNA repair enzymes. *J. Chem. Phys.*, **129**, 235101.

Fok, P.-W. & Chou, T. (2010) Reconstruction of potential energy profiles from multiple rupture time distributions. *Proc. R. Soc. A, Math. Phys. Eng. Sci.*, **466**, 3479–3499.

Freund, L. B. (2009) Characterizing the resistance generated by a molecular bond as it is forcibly separated. *Proc. Natl Acad. Sci. USA*, **106**, 8818–8823.

Gardiner, C. W. (1985) *Handbook of Stochastic Methods*. Berlin: Springer.

Giraudo, M. T. & Sacerdote, L. (1999) An improved technique for the simulation of first passage times for diffusion processes. *Commun. Stat. - Simul. Comput.*, **28**, 1135–1163.

Giraudo, M. T., Sacerdote, L. & Zucca, C. (2001) A Monte Carlo method for the simulation of first passage times of diffusion processes. *Methodol. Comput. Appl. Probab.*, **3**, 215–231.

Goldstein, S. (1951) On diffusion by discontinuous movements and on the telegraph equation. *Q. J. Mech. Appl. Math.*, **4**, 129–156.

Hummer, G. & Szabo, A. (2003) Kinetics from nonequilibrium single-molecule pulling experiments. *Biophys. J.*, **85**, 5–15.

Kress, R. (1989) *Linear Integral Equations*. Berlin: Springer.

Mannella, R. & Palleschi, V. (1989) Fast and precise algorithm for computer simulation of stochastic differential equations. *Phys. Rev. A*, **40**, 3381–3386.

Masoliver, J. & Weiss, G. H. (1994) Telegrapher's equations with variable propagation speeds. *Phys. Rev. E*, **49**, 3852–3854.

Novikov, R. G. (1994) The inverse scattering problem at fixed energy for the three-dimensional Schrödinger equation with an exponentially decreasing potential. *Commun. Math. Phys.*, **161**, 569–595.

Sacks, P. & Symes, W. (1987) Recovery of the elastic parameters of a layered half-space. *Geophys. J. R. Astron. Soc.*, **88**, 593–620.

Symes, W. W. (1991) A differential semblance algorithm for the inverse problem of reflection seismology. *Comput. Math. Appl.*, **22**, 147–178.

Taillefumier, T. & Magnasco, M. O. (2010) A fast algorithm for the first-passage times of Gauss–Markov processes with Hölder continuous boundaries. *J. Stat. Phys.*, **140**, 1130–1156.

Trefethen, L. N. (2000) *Spectral Methods in Matlab*. Philadelphia: SIAM.

Appendix A. Derivation of a multi-state Broadwell process

A 1D generalized Broadwell model describes a particle that can take any one of K states. Initially, the particle is at position x and in state i. A particle in state $1 \leqslant k \leqslant K$ advects within an interval $(-L/2, L/2)$ with a velocity function $v_k(y)$ that is single signed for each k on $-L/2 \leqslant y \leqslant L/2$ with y being the current position. While advecting, the particle may transition from state i to any other state j with probability $F_{ji}(y)\mathrm{d}t$ within time interval $(t, t + \mathrm{d}t)$. Also $F_{ji}(y)$ are positive functions when $i \neq j$, but $F_{ii}(y) \equiv 0$. The goal of this appendix is to find the backward equation for the exit time distribution for such a process.

If $P(y, k, t \mid x, i, 0)\mathrm{d}y$ is the probability that the particle lies between y and $y + \mathrm{d}y$ and is in state k at time t, given that it had started at position x in state i at time $t = 0$, the Chapman–Kolmogorov equation (Gardiner, 1985) is

$$P(y, k, t + \mathrm{d}t \mid x, i, 0) = \sum_{j=1}^{K} \int_{V_1 \mathrm{d}t}^{V_2 \mathrm{d}t} P(y, k, t + \mathrm{d}t \mid x + \xi, j, \mathrm{d}t) P(x + \xi, j, \mathrm{d}t \mid x, i, 0)\, \mathrm{d}\xi, \qquad (A.1)$$

where $V_1 = \min_k \min_{-L/2 < y < L/2} v_k(y)$, $V_2 = \max_k \max_{-L/2 < y < L/2} v_k(y)$ and state k and position y of the particle at time $t + \mathrm{d}t$ arise from accounting for all transitions from intermediate states j, $j = 1, \ldots, K$
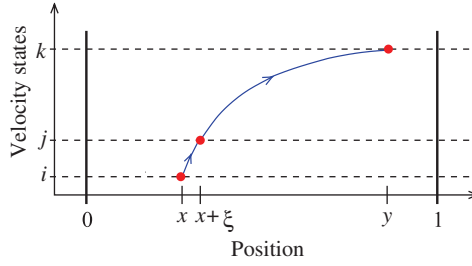
FIG. A1. The transitions relevant for computing the Backward equation for the probability density of a multi-state persistent random walk. The quantities x, $x + \xi$ and y represent initial, intermediate and final positions while i, j and k represent initial, intermediate and final states.

and positions $x + \xi$ at time dt; see Fig. A1. Note that V_1 can be negative and the integration over $V_1 \, \mathrm{d}t < \xi < V_2 \, \mathrm{d}t$ corresponds to all possible displacements from position x.

We will assume that the advection velocities and flip rates are explicitly time-independent so that the process is time-homogeneous. Therefore, the probabilities are time-translationally invariant and $P(y, k, t + \mathrm{d}t \mid x + \xi, j, \mathrm{d}t) = P(y, k, t \mid x + \xi, j, 0)$. In the following calculations, we make frequent use of delta distributions, so Taylor expansions and associated derivatives are to be interpreted in the weak sense.

The probability of transition from (x, i) to $(x + \xi, j)$ in time dt can be decomposed into two terms corresponding to continued particle advection when no state flips occur in time dt, or a state change occurring within $(0, \mathrm{d}t)$:

$$P(x + \xi, j, \mathrm{d}t \mid x, i, 0) = \delta(\xi - v_i(x) \, \mathrm{d}t) \left(1 - \sum_{\substack{\ell=1 \\ \neq i}}^{K} F_{\ell i}(x) \, \mathrm{d}t \right) \delta_{ij} + \delta(\xi) F_{ji}(x)(1 - \delta_{ij}) \, \mathrm{d}t + \mathrm{O}(\mathrm{d}t^2).$$

$$(\mathrm{A}.2)$$

The symbols δ_{ij} and $\delta(\cdot)$ denote the usual Kronecker tensor and Dirac delta function, respectively. The first term in (A.2) represents the probability that the particle did not transition out of state i in $(0, \mathrm{d}t)$, while the second term describes the transition probability from state i to state $j \neq i$.

In (A.2), when $i = j$, the term proportional to F_{ji} is zero (no state transitions have occurred) and the probability density originally centred at x is simply advected to $x + v_i(x) \, \mathrm{d}t$. Therefore, the probability density of being in position $x + \xi$ and state $j = i$ at time dt is $\delta(\xi - v_i(x) \, \mathrm{d}t)(1 - \sum F_{\ell i}(x) \, \mathrm{d}t)$. When $i \neq j$, the term proportional to $1 - \sum F_{\ell i} \, \mathrm{d}t$ is zero. To $\mathrm{O}(\mathrm{d}t)$, we can ignore advection and simply assume the particle changed state in its current position.[1] Therefore, the probability of being at position $x + \xi$ and state j at time dt is $\delta(\xi) F_{ji}(x) \, \mathrm{d}t$.

Upon Taylor-expanding the remaining probability densities in (A.1),

$$P(y, k, t + \mathrm{d}t \mid x, i, 0) = P(y, k, t \mid x, i, 0) + \frac{\partial P}{\partial t} \, \mathrm{d}t + \mathrm{O}(\mathrm{d}t^2), \tag{A.3}$$

$$P(y, k, t \mid x + \xi, j, 0) = P(y, k, t \mid x, j, 0) + \frac{\partial P}{\partial x} \xi + \mathrm{O}(\xi^2), \tag{A.4}$$

---

[1] If advection was included, $\delta(\xi) F_{ji} \, \mathrm{d}t$ in (A.2) would be replaced with $\delta(\xi + \mathrm{O}(\mathrm{d}t)) F_{ji} \, \mathrm{d}t$ corresponding to an additional displacement of $\mathrm{O}(\mathrm{d}t)$ and an associated error of $\mathrm{O}(\mathrm{d}t^2)$.

we find to order dt (note that $\xi = \mathrm{O}(\mathrm{d}t)$),

$$\frac{\partial}{\partial t} P_{ki}(y, t \mid x, 0) = \sum_{j=1}^{K} L_{ji} P_{kj}(y, t \mid x, 0), \tag{A.5}$$

where

$$P_{ki}(y, t \mid x, 0) \equiv P(y, k, t \mid x, i, 0), \quad L_{ji} = \delta_{ij} v_i(x) \partial_x + (1 - \delta_{ij}) F_{ji} - \delta_{ij} \sum_{\substack{\ell=1 \\ \neq i}}^{K} F_{\ell i}. \tag{A.6}$$

When $t \leqslant 0$, the particle is at $y = x$ in state i so that

$$P(y, k, t \mid x, i, 0) = \delta_{ik} \delta(x - y), \quad t \leqslant 0. \tag{A.7}$$

Henceforth, we consider the domain $y \in (-L/2, L/2)$ with absorbing boundaries at $y = \pm L/2$ so that, when $t > 0$, the appropriate boundary conditions are

$$\begin{aligned} P(y, k, t \mid x = +L/2, i, 0) &= 0 \quad \forall i : v_i > 0, \\ P(y, k, t \mid x = -L/2, i, 0) &= 0 \quad \forall i : v_i < 0. \end{aligned} \tag{A.8}$$

A.1 *Survival probabilities*

If we do not distinguish from which boundary the particle eventually exits, we can define the survival probability by integrating (A.5) over all positions $y \in (-L/2, +L/2)$ and summing over all possible final states. The survival probability

$$S_i(x, t) = \sum_{k=1}^{K} \int_{-L/2}^{L/2} P(y, k, t \mid x, i, 0) \, \mathrm{d}y, \tag{A.9}$$

describes the probability that a particle started at position $x \in (-L/2, +L/2)$ in state i has not left through either boundary up to time t. When $t \leqslant 0$, we have, from (A.7),

$$S_i(x, t) = 1, \quad -L/2 \leqslant x \leqslant L/2. \tag{A.10}$$

When $t > 0$, the survival probability obeys

$$\frac{\partial}{\partial t} S_i(x, t) = v_i(x) \frac{\partial}{\partial x} S_i(x, t) + \sum_{\substack{j=1 \\ \neq i}}^{K} F_{ji}(x) S_j(x, t) - \sum_{\substack{\ell=1 \\ \neq i}}^{K} F_{\ell i}(x) S_i(x, t), \tag{A.11}$$

with boundary conditions

$$\begin{aligned} S_i(L/2, t) &= 0 \quad \text{for } i : v_i(x) > 0, \\ S_i(-L/2, t) &= 0 \quad \text{for } i : v_i(x) < 0. \end{aligned} \tag{A.12}$$

A.2 *Exit time distributions*

The full exit time distribution is found from the usual definition $w(t \mid x, i, 0) \equiv w_i(x, t) = -\partial S_i(x, t)/\partial t$, and so, differentiating (A.11), we have

$$\frac{\partial}{\partial t} w_i(x, t) = v_i(x) \frac{\partial}{\partial x} w_i(x, t) + \sum_{\substack{j=1 \\ \neq i}}^{K} F_{ji}(x) w_j(x, t) - \sum_{\substack{\ell=1 \\ \neq i}}^{K} F_{\ell i}(x) w_i(x, t). \qquad (A.13)$$

The initial condition is found by differentiating (A.10) in time so that $w_i(x, t) = 0$ when $t \leqslant 0$. In particular,

$$w_i(x, 0) = 0. \qquad (A.14)$$

From (A.11) and (A.12), we have $S_i(L/2, t) = S_i(-L/2, t) = H(-t)$ for all t. Therefore, the boundary conditions for $w_i(x, t)$ are

$$\begin{aligned} w_i(L/2, t) &= \delta(t) \quad \forall i : v_i > 0, \\ w_i(-L/2, t) &= \delta(t) \quad \forall i : v_i < 0. \end{aligned} \qquad (A.15)$$

When $K = 2$, $F_{12}(x) = F_{21}(x) = F(x)$, $v_1(x) = -v_2(x) = v$ (a positive constant), (A.13–A.15) reduce to (1–4).